Penn Array Receiver

Penn Array Receiver CDR Document 4:
Detailed Design Documents

Contents

A high capacity 250 mK ^{3}He/^{4}He refrigeration system based on a pulse tube cooler.

M.J. Devlin, S.R. Dicker*, J. Klein, M.P. Supanich

University of Pennsylvania, Philadelphia, USA

Abstract

We present the design of a completely closed-cycle refrigeration system. The system consists of four stages; the first two, 40.5 K and 2.7 K, are provided by a pulse tube cooler, the third and fourth stages by helium adsorption refrigerators. The adsorption refrigerators use ^{4}He and ^{3}He with base temperatures of 700 mK and 250 mK respectively. With a load of 15 μK, a temperature below 286 mK can be maintained for 72 hours.

Key words: cryogen-free, ^{3}He adsorption refrigerator, pulse tube cooler

1 Introduction

The next generation of facility instruments for mm-wave telescopes will use arrays of bolometric detectors cooled to below 300 mK. Such Facility instruments must have long hold-times and require little or no operator intervention. We are constructing a 90 GHz receiver containing 64 TES detectors (see Benford et al.[1] for details of these detectors). The receiver will be placed on the new 100 m diameter Green Bank Telescope[1] (GBT) in West Virginia, USA [2].

Up to 8 receivers on the GBT are housed on a rotating turret which allows the telescope to switch operating frequencies without down-time. The turret housing is located at the secondary focus 135 m above the ground and is inaccessible during operation. It can tilt between -13° and +72° from the horizontal (corresponding to observing angles of 90° and 5° above the horizon). Because the turret rotates mounting a receiver at an angle will not ensure it stays within ±45° of the horizontal so any receiver must be able to withstand

* corresponding author

[1] see http://www.gb.nrao.edu/GBT/GBT.shtml

being tipped by 72° in any direction. The refrigeration system described in this paper was designed to provide cooling for our array on the GBT.

2 System Requirements

The following list of requirements was determined based on telescope and observing restrictions.

- The system must provide 15 μW of cooling at temperatures below 290 mK maintained at angles of at least 57° from the vertical (corresponding to observations 20° above the horizon). Due to atmospheric opacity, observations less than 20° above the horizon are restricted consequently full cooling capacity is not needed.
- When the receiver is not in use it may be tipped by up to 72° in any direction and after this it must be ready to use within 90 minutes of being returned upright.
- To allow for deep observations, the receiver must stay cold for over 24 hours at a time.
- The receiver must be operated remotely by members of the astronomical community who are not familiar with cryogenics.

The system described below meets each of these requirements.

3 System overview

An outline of our system is shown in Figure 1. There are four temperature stages, the first two, at 40.5 K and 2.7 K are provided by a pulse tube cooler, the third stage is a ^{4}He adsorption refrigerator, and the fourth stage is a ^{3}He adsorption refrigerator. The following sections cover each of these stages.

3.1 The pulse tube cooler

Expendable liquid cryogens are impractical on the GBT. Access to the receiver is limited, replenishing cryogens would be prohibitively difficult. Other GBT receivers are cooled (to 15 K) using closed cycle Gifford-McMahon (GM) cryocoolers. The high pressure helium required by such cryocoolers is supplied by compressors located at the base of the telescope. There are several commercial cryocoolers capable of cooling to below 4 K including the PT405 made by

Cryomech [2], a two stage pulse tube cooler[3] with a cooling capacity of 30 W and 0.5 W at 55 K and 4.2 K respectively. Base temperatures around 2.6 K are achieved. Unlike GM cryocoolers, pulse tubes have no mechanical displacers so wear on seals and the vibrations associated with GM cryocoolers are reduced. However the PT405 is designed to operate vertically. At operating angles $>30^\circ$ from the vertical its capacity is reduced. We have investigated this effect on the performance of the entire system, and have found it to be acceptable down to $57^\circ$from the vertical.

3.2 The adsorption refrigerators

Adsorption refrigerators have three parts; a pump filled with a sorbent material, a cooled condensation point, and an evaporator (which can also be the condensation point). These elements are connected by a tube of low thermal conductivity and filled with gas, in this case ^{3}He or ^{4}He. To operate the refrigerator the helium is liquefied by cooling the condensation point to below the critical temperature of helium while keeping the pump above $\sim$25 K – hot enough to prevent helium being adsorbed by the sorbant material. The pump is then cooled via a heatswitch and it adsorbs the gaseous helium, lowering the pressure in the evaporator. The helium cools until its vapor pressure is equal to the pressure in the evaporator, then the refrigerator will stay at this temperature until all the helium has evaporated. At this point the pump is heated up so as to desorb the helium and the cycle is repeated.

The condensation efficiency in a adsorption refrigerator is a strong function of the condensation temperature. For the ^{3}He refrigerator described in this paper simple calculations which assume equilibrium is reached before the charcoal is cooled were carried out. These showed that if the charcoal is cooled with the the condensation point at 3 K, by the time the evaporator has cooled below 0.3 K, less than 23% of the ^{3}He is left as liquid. Cooling the condensation point to 1.2 K condenses 96% of the available helium and by the time it has cooled to 0.3 K over 80% is left as liquid and is available for cooling the detectors. Although the PT405 could in principle cycle a ^{3}He refrigerator, in practice the extra load from the ^{3}He refrigerator would warm the 2nd stage of the PT405 above 3 K. Efficient cycling of ^{3}He adsorption refrigerators from the 2nd stage of the PT405 is not possible.

To overcome this, a ^{4}He adsorption refrigerator was added between the pulse tube and the ^{3}He refrigerator's condenser. Simple models for our ^{4}He adsorption refrigerator predicted that even with a condenser at 3.5 K, 91.5% of the ^{4}He gas would condense and after cooling to 0.8 K over 70% would still remain

[2] see http://www.cryomech.com

as liquid. Once cycled, the ^{4}He stage is then used to cool and condense the ^{3}He gas in the ^{3}He stage.

4 Detailed design

A cross-section of the ^{3}He and ^{4}He refrigerators is shown in Figure 1. By designing the refrigerators as separate units that bolt together construction was simplified and in the future it will be possible to use one stage without the other.

4.1 The ^{4}He refrigerator

The ^{4}He refrigerator is assembled around a piece of thin-walled 316 stainless steel tubing. The condenser, which also acts as the mounting point for the refrigerator, is an OFHC coper disk silver soldered approximately halfway down the tube. The evaporator has an OFHC copper bottom with concentric rings cut on the inside so as to decrease the effect of thermal boundary (Kapitza) resistance.

The pump is a stainless steel cylinder filled with OFHC copper fins which make thermal contact to the activated charcoal[4] which is used as the sorbant material. The fins are joined to a copper plug in the wall of the pump to which a resistive heater and a thermometer are attached. The capacity of the ^{4}He refrigerator (28 S.T.P. liters gas) was designed to be enough to cycle the ^{3}He stage and provide 50 J of additional cooling. The amount of charcoal in the pump is set to be enough to adsorb all the helium with a safety margin of 2[5]. To ensure efficient recycling the whole refrigerator is filled to 500 psi (at 300 K).

To connect the charcoal pumps to the PT405, solid state, mechanical and gas-gap heatswitches were considered. Mechanical heatswitches have the advantages of a very high on/off ratio and that power is only required to change the state of the switch. However these devices tend to be bulky and they require high current leads to drive the motor. Most importantly they are more prone to failure than the other options. Solid state heatswitches have the advantage of being totally passive devices, however high on/off ratios are hard to achieve. If used they would give either an unacceptably high load on the PT405 or result in a long cool-down time when cycling the refrigerator. Gas-gap heatswitches[6] can be run using low current wiring and are very reliable. Although $\sim$2 mW of power must be applied in order to keep them on, with a closed cycle system this is not a consideration. For these reasons we chose

gas-gap heatswitches to run the refrigerators[3].

Superfluid ^{4}He can climb the walls of the evaporator and travel up the pump tube where it evaporates. This flow can easily be the equivalent of 1–2 mW additional parasitic load on the evaporator (compared to 70 μW from thermal conduction down the pump tube). If the ^{4}He stage was to be used only to cycle the ^{3}He refrigerator, then this would not be a problem, however we require a temperature stage between the pulse tube and the ^{3}He refrigerator (to cool additional cold optics and reduce the loading on the ^{3}He stage). Other projects [7] have used an additional ^{3}He stage but this was ruled out for cost and simplicity reasons.

To reduce the superfluid leak we use a thin diaphragm with a 1.54 mm hole in it at the exit of the evaporator. Using the highest measured superfluid leak rate in the literature [8] we calculated the small circumference of the hole should restrict the superfluid leak to less than 0.1 mW. At the same time it is important for the hole to be big enough not to restrict the flow of gas from the evaporator to the charcoal pump. Gas flow in the pump tube is difficult to model as it is in the transition regime between laminar and molecular flow and the temperature is unknown. However, a range of models including some based on results scaled from our earlier ^{3}He refrigerators all showed that with 9 mW load, the ^{4}He evaporator should be below 1 K and > 30 mW is needed to heat the evaporator above 1.3 K.

4.2 The ^{3}He refrigerator

The ^{3}He refrigerator is of very similar design to the ^{4}He stage with two important differences. First, ^{3}He does not become superfluid until below 2 mK, so the diaphragm is not needed. Secondly, there is an extra heat exchanger between the condenser and the charcoal. During cycling ^{3}He gas leaving the charcoal is precooled by the second stage of the PT405 before reaching the condenser. This reduces the amount of ^{4}He needed to condense the ^{3}He by a factor of approximately 6. The overall design has been scaled to hold 6.15 S.T.P. liters ^{3}He gas at a pressure of 500 psi (at 300 K). Again a high pressure ensures efficient cycling. Models predict that if the refrigerator is cycled with the condenser at 0.7 K, 5.65 J of cooling should be available, with a cycling efficiency of 90%.

[3] Chase Research : model #CR-GHS-005

5 Cycling procedure

Figure 2 shows a typical cycle. The data were taken using ROX resistance thermometers [4] measured using a scanning resistance bridge controlled via the GPIB bus by a Labview program. The same Labview program also controls the heatswitches and the heaters on the charcoal pumps. When the cycle is started power to both heatswitches is turned off. As the response of the gas-gap heatswitches is not instantaneous, there is a 5 minute delay before 1.6 W and 0.2 W are applied to the ^{4}He and ^{3}He charcoal pumps respectively. These powers are left on until the charcoal has reached predetermined temperatures; 35 K for ^{3}He and 50 K for ^{4}He. These temperatures were chosen empirically to give a quick, efficient cycle. The program then waits until the ^{4}He evaporator cools to 3.5 K before applying power to close the ^{4}He charcoal heatswitch and to cool the ^{4}He refrigerator. The program then waits for the ^{3}He evaporator to cool to 0.75 K before closing the ^{3}He heatswitch and completing the cycle. Typically the whole process takes 4.5 hours and is limited by how long it takes to remove energy through the second stage of the PT405. The installation of a better thermal link or a more powerful cryocooler would speed up this process. No fine tuning of thermal loads or thermal links was needed.

This cycling procedure has been shown to be robust and efficient in condensing the helium. Because the procedure waits for the evaporator to cool to preset values (rather than waiting for set amounts of time) it works with the PT405 tipped by 45 degrees where its cooling power is greatly reduced.

6 Performance

6.1 The ^{4}He system

The ^{4}He refrigerator cools to a base temperature of 700 mK and is stable to better than 0.1 mK on time scales between 0.25 seconds and 10 minutes. Slow drifts up to 0.4 mK/hour where sometimes observed on longer time scales. For our application such drifts do not pose a problem. Typical cycles were shown to condense the expected amount of ^{4}He; 75 J, of which 55 J are left if the ^{3}He refrigerator is cycled. The load curve (figure 3) shows that for an applied power of 10 mW the evaporator is at 1 K, demonstrating that the diaphragm does not adversely affect the flow of gas. At higher powers the slope of the load curve starts to increase again. We attribute this to the charcoal pump being heated by the adsorption of the helium to the extent that it looses some

[4] Lakeshore Cryogenics part #RX-202A-AA-M

of its efficiency. A better heatswitch would improve this situation.

If not used to cycle the ^{3}He refrigerator the ^{4}He refrigerator has a hold time of 24 hours. This corresponds to a parasitic load of 790 μW , significantly more than that expected due to conduction down the pump tubes (70 μW) and the superfluid leak (90 μW). The cause of this extra load is under investigation. There is a strong possibility of oxidization around the hole in the diaphragm. The thickness of a superfluid film is highly dependent on surface conditions so an oxide layer could increase film thickness and increase the superfluid leak rate.

6.2 The ^{3}He system

The ^{3}He refrigerator achieved a base temperature of 250 mK. After cycling, the refrigerator quickly cools below 290 mK. There is then a period of 1–2 hours while the temperature of the refrigerator stabilizes. The final temperature stability is $\pm$90 μK on time scales between 0.25 seconds and 10 minutes. Long term drifts drop below 0.2 mK/hour.

With a 15 μW load the ^{3}He refrigerator had a hold time of 72 hours - far longer than the ^{4}He refrigerator. However, load curves of the ^{3}He refrigerator (Figure 4) show operating temperatures (under 15 μW of loading) of 270 mK and 286 mK when the ^{4}He refrigerator is at 700 mK and 2.8 K respectively. This more than meets our cooling requirements allowing the entire 72 hour hold time to be used, giving the system a 94% duty cycle. The change in the base temperature when the ^{4}He refrigerator runs out is that expected due to the increased thermal conductance up the pump tube.

6.3 The response to tilt

To test the response of the system to tilt, the system was left at 57° (the limit of useful observations) and 72° (the hard limit of the telescope) from vertical for several hours, being returned vertical between each test. The behavior and recovery of the system was monitored. In addition, load curves of the ^{3}He refrigerator were taken at a range of angles. At 57° the efficiency of the first stage of the pulse tube drops rapidly and over two hours it warmed to 70 K. The second stage was relatively unaffected showing only a rapid warming to 3.4 K before becoming stable. Both the ^{3}He and ^{4}He stages were unaffected.

On tilting to 72° the second stage of the pulse tube warms to about 20 K in an hour. Because the charcoal pumps become hot the adsorption refrigerators no longer work. On tilting back to vertical the system recovers in less than 40

minutes. Such extreme tilting often acted to partly cycle the ^{4}He refrigerator. So far, no effects on the hold-time of the ^{3}He system have been seen.

Load curves of the ^{3}He refrigerator taken at different angles show little dependence on angle up to 30° (figure 5) (the maximum tested). This fact and that no increase in base temperature over the hold time of the refrigerators was observed demonstrates Kapitza resistance is not a problem. Calculations using the surface area of copper fins inside the evaporator in contact with the liquid helium provide confirmation of this result.

7 Conclusions

The refrigeration system we have designed and built has been shown to meet all our requirements for the Green Bank Telescope. Without using expendable cryogens, the system reaches a base temperature of 250 mK and can cool to 286 mK with loads of 15 μW and hold times of over 70 hours. This design should be easy to scale to other experiments.

8 Acknowledgments

This work was built on earlier work carried out by Jason Puchalla and we are grateful for his help. Funding was provided from the National Radio Astronomy Observatory who run the Green Bank observatory and Mark Devlin's NFS career grant number AST97-32960.

References

[1] Benford DJ, Chervenak JA, Irwin KD, Moseley HS. Ultralow-Background Large-Format Bolometer Arrays. SPIE 2003;4850:944–953

[2] Prestage RM, Maddalena R. Green Bank Telescope: status and early results. In Proceedings of SPIE Vol. 4837 Eds Oschmann JM, Stepp LM, 2002, In press.

[3] Radebaugh R. A review of pulse tube refrigeration. In Advances in cryogenic engineering Vol 35B, Plenum Press, 1990.p.1191–1205

[4] Charcoal supplied by Calgon Carbon, Pittsburg, USA: OVC 4×8 Coconut-based activated charcoal.

[5] Sedgley DW, Tobin AG, Batzer TH, Call WR. Characterization of charcoals for helium cryopumping in fusion devices. J. Vac. Sci. Technol. 1987;5:2572–2576

[6] Frank DJ, Nast TC. Getter-activated cryogenic thermal switch. Adv. Cry. Eng. 1986;31:933–940

[7] Bhatia RS, Chase ST, Edgington SF, Glenn J, Jones WC, Lange AE, et al. A three-stage helium sorption refrigerator for cooling of infrared detectors to 280 mK. Cryogenics 2000;40(11):685–691

[8] Herbert GR, Chopra KL, Brown JB. Helium film flow below 1°K. Phys Rev, 1957;106:391–393

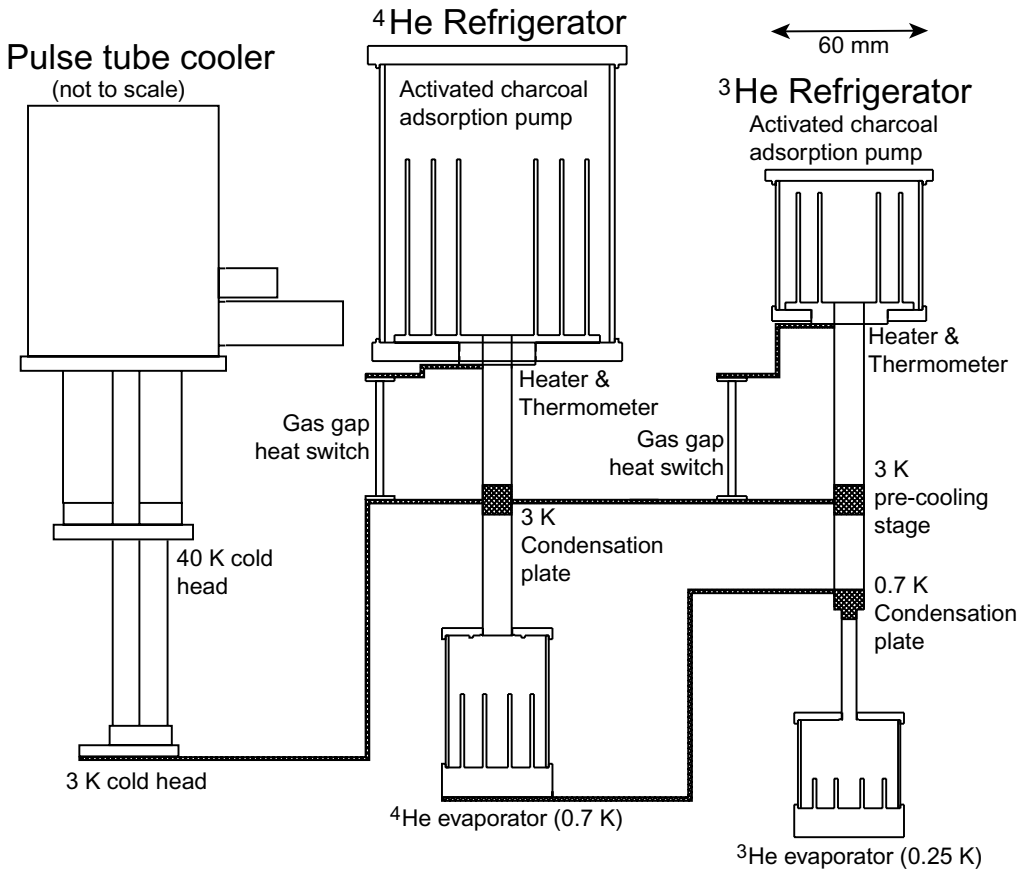

Fig. 1. A schematic of our cryogenic system and how the different stages are connected.

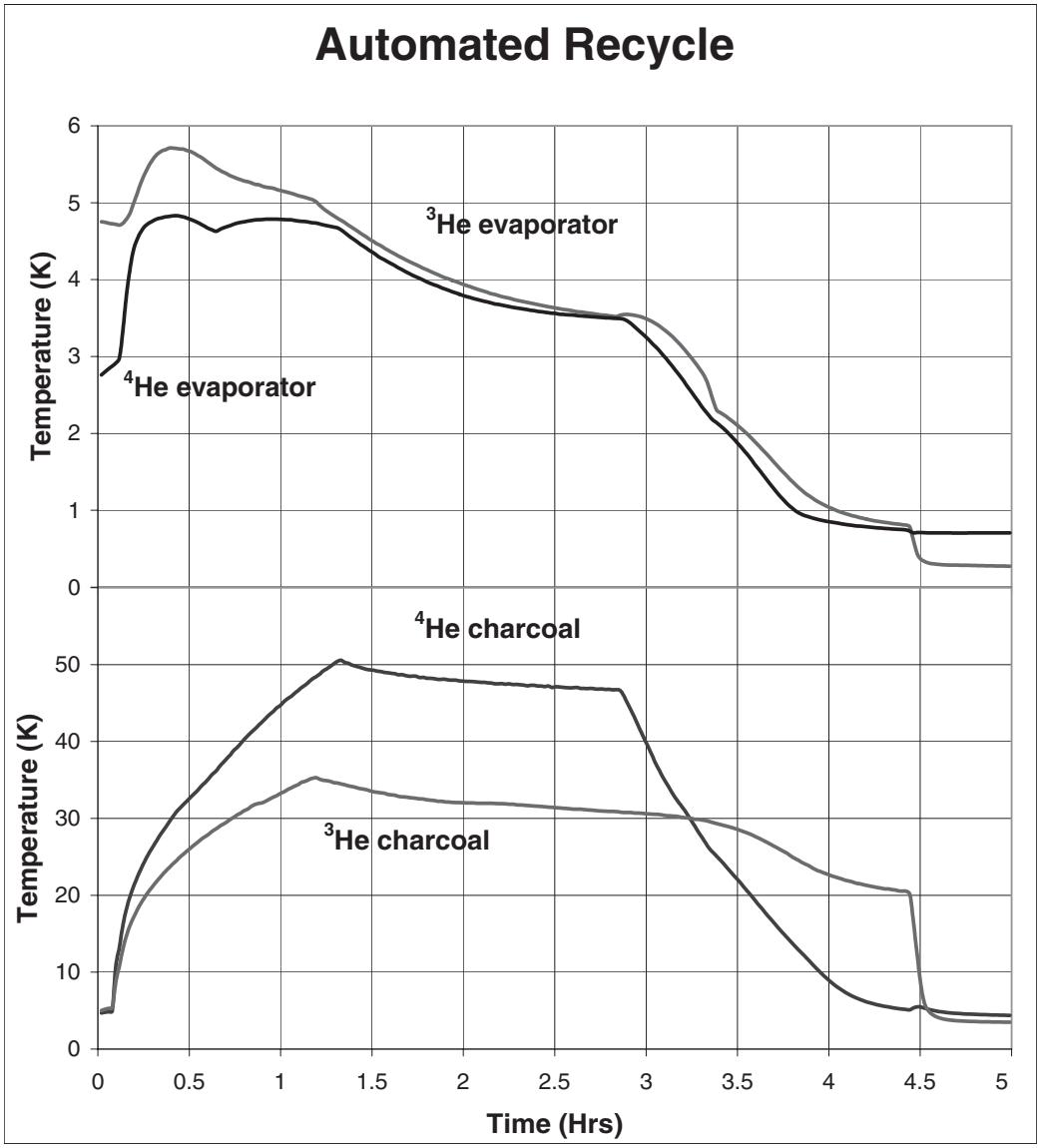

Fig. 2. A typical automated cycle of both adsorption refrigerators. At 0:00 the heatswitches were turned off and at 0:05 1.6 W and 0.2 W was applied to heat the ^{4}He and ^{3}He charcoal. At 1:20 the heaters are turned off and at 2:51 the ^{4}He has condensed and cooled to 3.5 K so the ^{4}He heatswitch is closed. At 4:24 the ^{3}He has condensed and the ^{3}He heatswitch is closed ending the cycle.

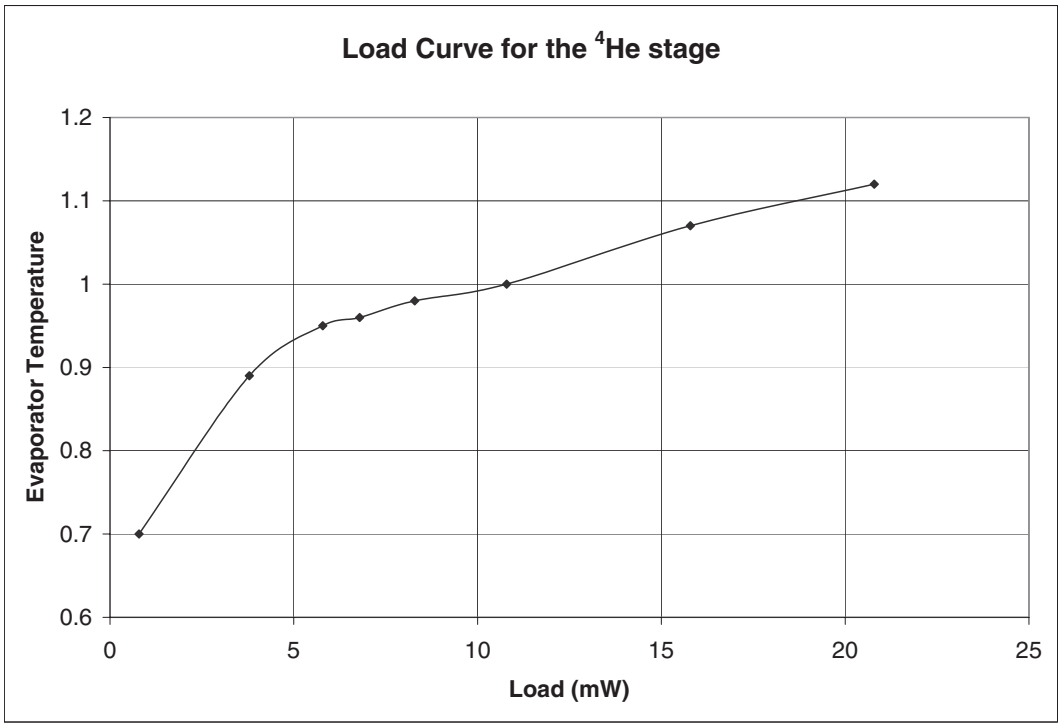

Fig. 3. The ^{4}He load curve. The flat response of this curve is confirmation that the diaphragm is not limiting the gas flow between the evaporator and the pump.

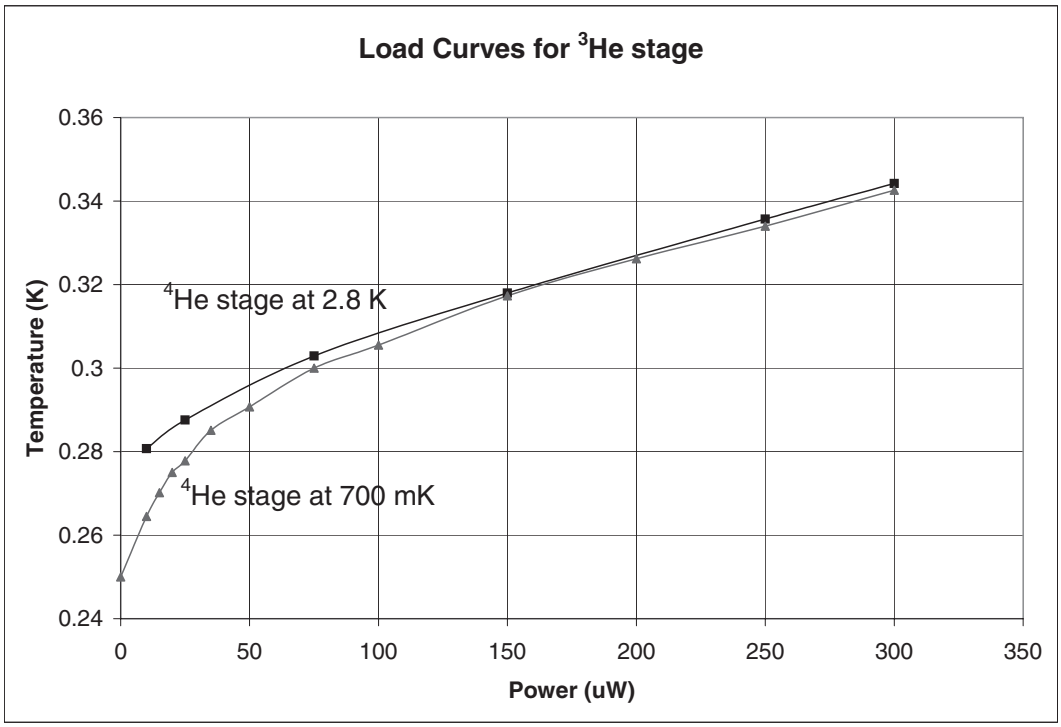

Fig. 4. Load curves for the ^{3}He refrigerator taken with the ^{4}He refrigerator at 700 mK and 2.8 K.

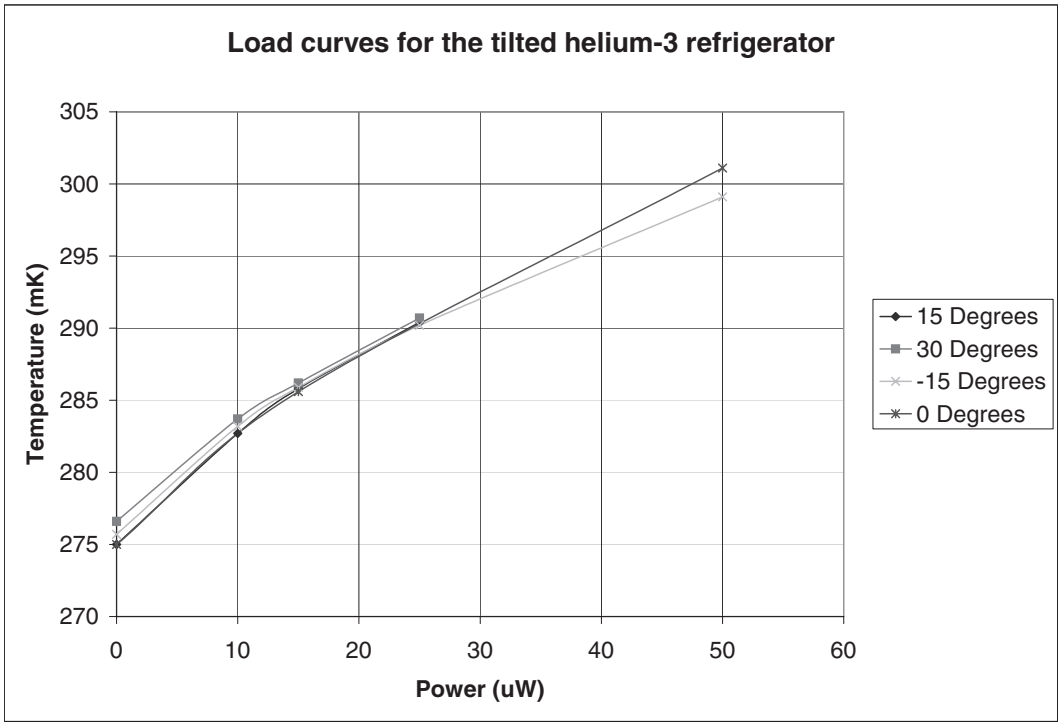

Fig. 5. Load curves for the ^{3}He refrigerator when tipped from the vertical and the ^{4}He refrigerator warm.

This page is blank

Summary of Cryostat Tests at Green Bank Sept '03

The tests described in the proceeding paper were carried out in the lab with just 20 feet of ¾ " helium lines connecting the compressor to the pulse tube. Tilt test were carried out manually. On the GBT there will be over 600 feet of ¾ " helium lines with extra fittings between the compressor and the pulse tube, there is a greater chance of contamination, the compressor will not be the same and motion of the telescope may be continuous. To test the performance of the cryostat under working conditions the test cryostat was placed in the receiver cabin of the GBT and ran overnight while low frequency observations were carried out.

The cryostat was operated with the compressor producing a supply pressure of 270 PSIG and a return pressure of 90 PSIG – slightly lower than the 310 PSIG supply and 110 PSIG return used at Upenn. With the receiver cabin horizontal the first stage of the pulse tube ran at 45 K, 5 K hotter than in the lab. The second stage ran at 2.9 K, only 0.2K higher than the lab – well within acceptable operating conditions.

An automatic recycle of the ^{4}He and ^{3}He stages was carried out with the receiver cabin horizontal. This took 5.5 hours, 1 hour longer than in the lab indicating slightly lower cooling capacity. It is worth noting that parasitic loading on the final cryostat is likely to be lower so this effect may cancel. Even with a 15 μW load on the ^{3}He evaporator, far higher than expected, this would give a 93% duty cycle.

Finally, with the cryostat and both refrigerators cold, the cryostat was monitored overnight while lower frequency observations were carried out. Plots of the stability of the pulse tube and sorption refrigerators against the elevation of the telescope are shown after this page. They show a good match to lab tests, with the performance of the1st stage of the PT405 declining rapidly below elevations of 30º. The ^{3}He stage was much more stable showing changes less than 2 mK at elevations less than 20° (while the ^{4}He refrigerator lasted). With the ^{4}He refrigerator empty the 3He stage showed 4 mK increases at elevations of 15°.

The temperature of the ^{3}He stage was 70 mK higher than in the lab and the data are much more noisy. If this increase were real the hold time of the refrigerator would have been less than 5 hours so we attribute this increase as an electronics problem. The long slow drifts in the ^{3}He temperature may be partly due to this problem too.

In conclusion we have demonstrated that our cryogenic system is expected to function as well on the GBT as in the lab, more than meeting our requirements.

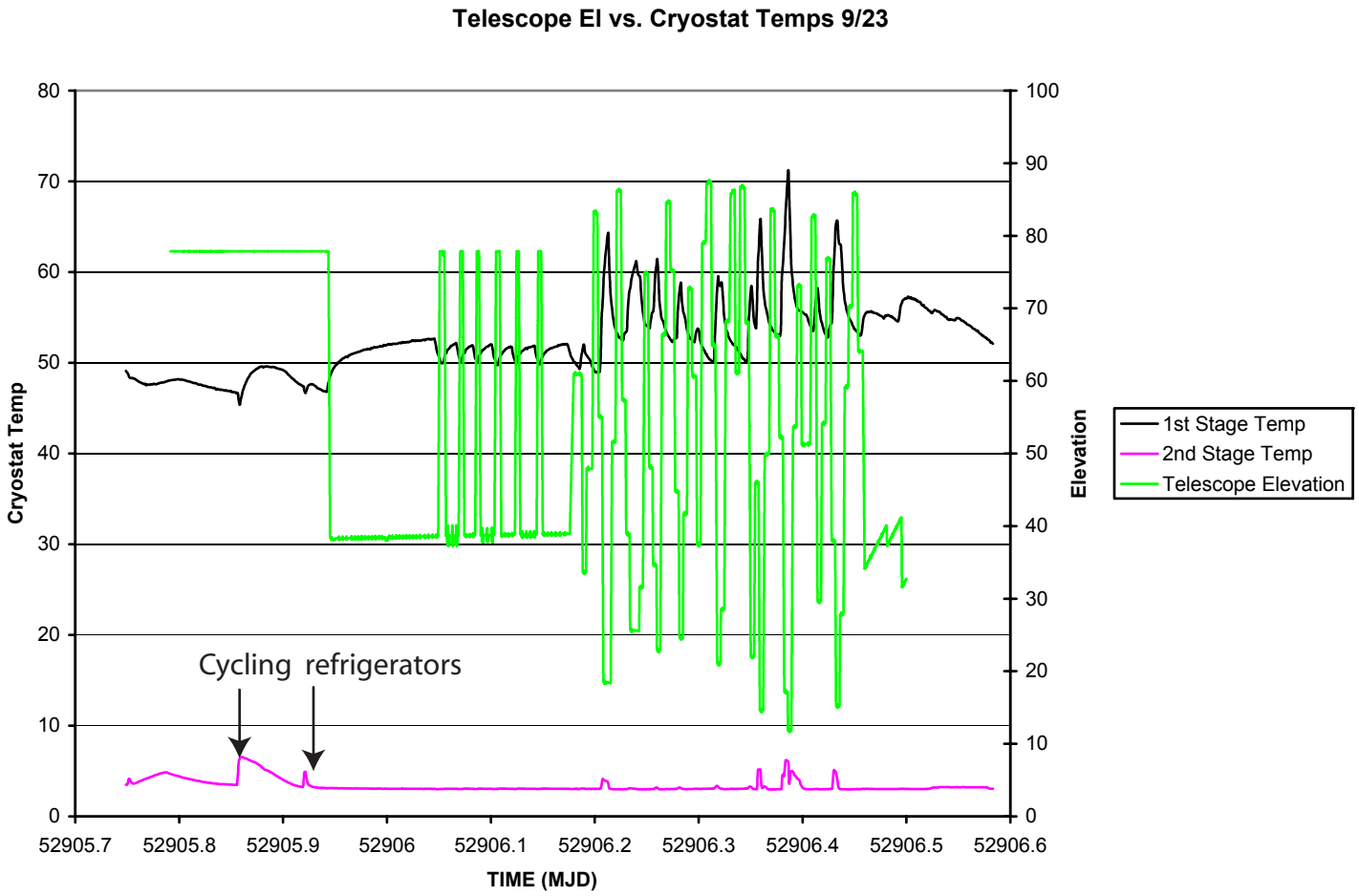
Telescope El vs. Cryostat Temps 9/23
Cryostat Temp
Elevation
TIME (MJD)
Cycling refrigerators
1st Stage Temp
2nd Stage Temp
Telescope Elevation
0
10
20
30
40
50
60
70
80
90
100
52905.7
52905.8
52905.9
52906
52906.1
52906.2
52906.3
52906.4
52906.5
52906.6

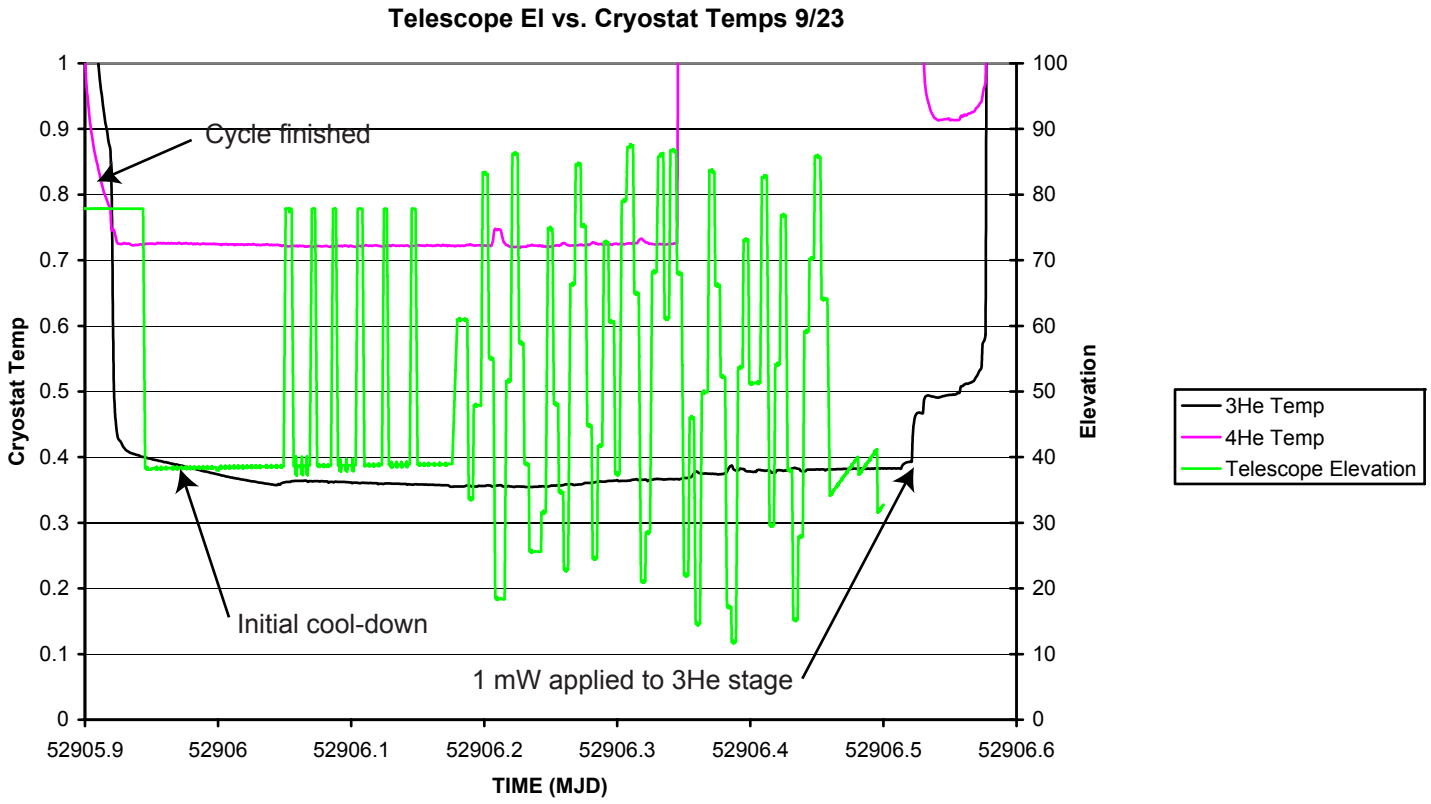
Telescope El vs. Cryostat Temps 9/23
Cycle finished
Initial cool-down
1 mW applied to 3He stage
Cryostat Temp
Elevation
TIME (MJD)
3He Temp
4He Temp
Telescope Elevation

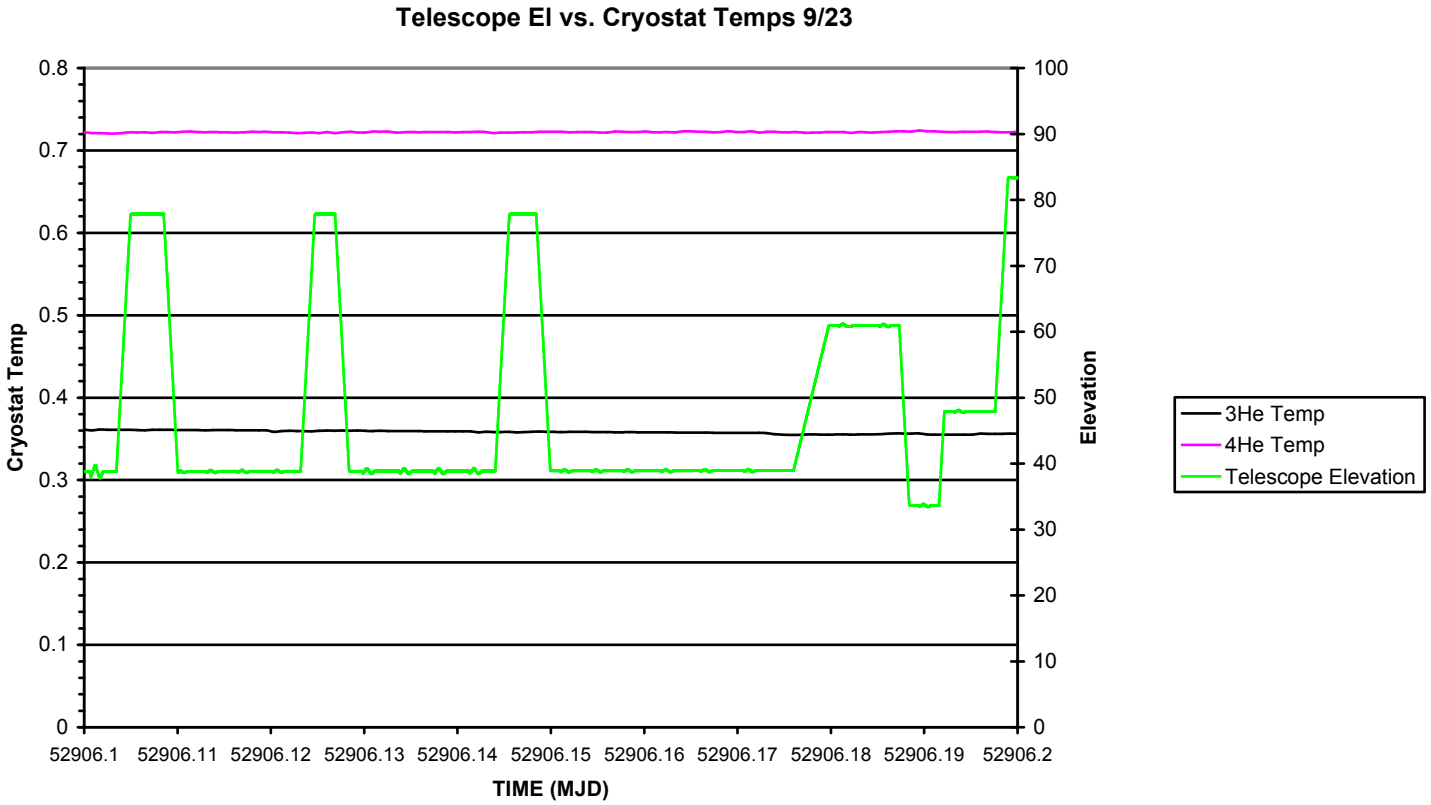
Telescope El vs. Cryostat Temps 9/23
Cryostat Temp
Elevation
TIME (MJD)
3He Temp
4He Temp
Telescope Elevation

This page is blank

Optics for the 90 GHz GBT array

Introduction

The 90 GHz array will have 64 TES bolometers arranged in an 8×8 square, read out using 8 SQUID multiplexers. It is designed as a facility instrument for the GBT telescope which is an off-axis Gregorian system. The primary mirror is a 100×110 m section of a 208 m diameter paraboloid with a 60 m focal length. The secondary is 8 m in diameter and is positioned at an angle of 5.57° to the vertex line. This tilt removes beam squint between polarizations at the Gregorian focual plane which is located at, and co-planar with, the roof of the receiver cabin; tilted by 12.329° with respect to the parent paraboloid. The 90 GHz array is designed for the Gregorian focus where the f# is 1.94. This document describes cooled optics designed to couple the TES detectors to the existing GBT optics.

The work was carried out using Code V optical design software and the solution is available in Code V native format (.len), as a sequence file (.seq), or (for those with Zemax) it may be translated into Zemax format (look at the directory Seq2ZMX). The files includes all telescope surfaces and except where stated all work was done using sources at infinity. Many of the tests are complex. Script files and even programs (in Code V's native language) have been written to carry them out. This way the tests are easily repeated on new designs

Requirements

The optical system for the GBT must:

- Produce a plate scale of 1.27 arcseconds/mm. This gives ~0.525fλ pixel spacing on the sky from the detectors which are spaced by 3.3 mm.
- Control the illumination of the secondary and primary mirrors.
- Keep optical loading on the cryogenics within acceptable limits; <100 mW @ 40 K; <10 mW @ 3 K; and <5 μW @ 0.3 K for the cryogenics)
- Keep optical loading on the detectors below 2 pW/detector
- Define a bandpass. For the first tests this should be 86—94 GHz.
- Flexibility is needed. In the future we may want to change bandpasses, detector spacing, or detector loading.

Size restrictions

The Gregorian receivers are mounted in a receiver cabin. The roof of the cabin rotates to allow any of 8 receivers to be moved into the secondary focus (Figure 1.). The receivers are lowered through circular holes and the 90 GHz array is assigned a 24 inch diameter hole. This puts a hard limit on the size of the cryostat of 23.75 inches (603 mm) with a goal of 20 inches (508 mm). This lower goal is to allow cables to be fed through and to keep weight down.

The detectors are cooled using a 2-stage pulse-tube (~40 and ~3 K) and helium-4 and helium-3 adsorption (~0.7 and ~0.3 K) refrigerators. These three objects (cylinders ~100 mm diameter), the detector electronics (~15×150×150 mm), and the optics must fit within the cryostat with at least 30 mm room for heat shields around the edges.

Final design

A schematic of the final design is shown in Figure 2. The overall length of the optics (focus to focus) is 390 mm and they are less then 150 mm in diameter. Some notes on different parts follow:

Bare arrays are used. To obtain the 1.27 plate scale, the final focus must be f1.62. Horns can not be used as they would physically overlap (or their apertures would be too small to allow 90 GHz light through) and illumination of the telescope is controlled with a cold Lyot stop.

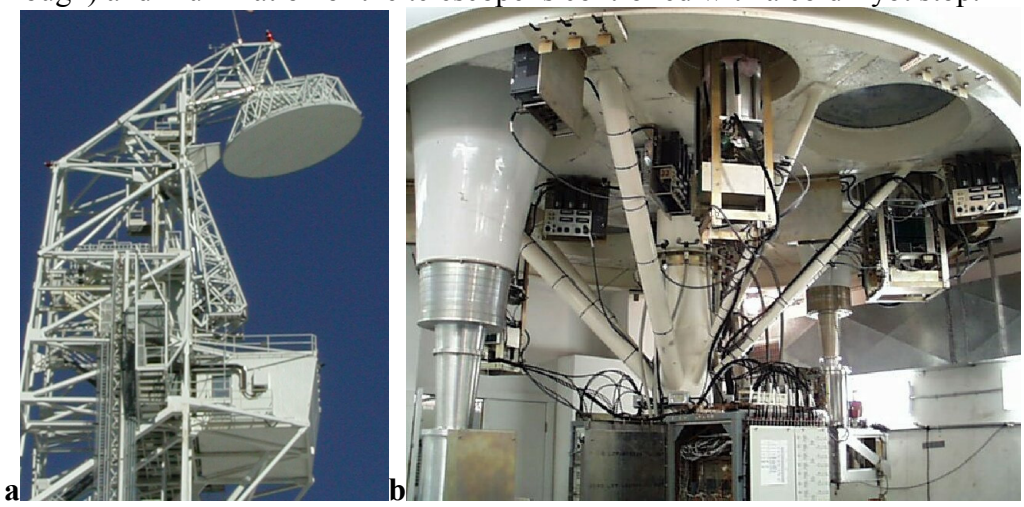

a **b**

Figure 1: **a** : The 8 m secondary mirror and receiver cabin seen from below. **b** : The inside of the receiver cabin showing the holes where the 90 GHz array must fit.

The Lenses

- Both lenses are 10th order aspheres. The use of aspheres increased off-axis image quality while maintaining a good Lyot stop.
- The lenses are diamond turned out of high purity, high resistivity silicon. This material is easy to obtain and its high refractive index means lenses can be thin. Silicon has very low loss at 90 GHz. Silicon also has good thermal conductivity and can act as a secondary IR blocker.
- Because of its high refractive index anti-reflective (AR) coating the lenses is required. Cardiff University has experience putting AR coatings on silicon. These coatings made of a plastic metal-oxide mixture, tailored to give the correct refractive index, require a 5 μm finish, easily obtainable with diamond turning.
- Image quality could be easier to obtain if lens 2 is reversed but this would lead to very bad ghosting (see below) so aspheric surfaces have been used to obtain image quality instead (see ghosting section below).
- The positions of the lenses have been chosen to match the heights of the temperature stages of the pulse tube to make installation easy.

Loading and bandpass filters

- To keep loading on the cryogenics to a minimum the cryostat window is placed close to the Gregorian focus (where it can be small).
- A reflecting capacitive mesh lowpass filter at 40 K (filter 1) keeps IR power from the colder stages where less cooling power is available. Neutral density filters can also be added at this location. This could become necessary if the atmospheric emission is greater than expected. By placing these filters near to the window they are smaller, making their manufacture easier and further reducing the amount of IR-power.
- Filter 2 is also a lowpass capacitive mesh filter designed to cut out the peak of the 40K black body spectrum and stop and leaks in filter 1. It's cut off frequency should be close to the top of the band but it need not be too sharp.

- Filter 3 is the capacitive mesh bandpass filter. Its leaks are cut out by filters 1 & 2. It is important in controlling the loading on the detectors. Without it, 3 K radiation from the Lyot stop would saturate the detectors. Filter 3 reduces this loading to 0.22 pW/detector.
- The total loading from the cold optics is estimated to be 0.43 pW, compared to 0.27 pW from the warm mirrors and 0.5—2.8 pW from the atmosphere.
- The radii of the apertures (apart from the Lyot stop) have been set, using geometric ray tracing, to 130% of the radii of the clear apertures needed to admit all the rays hitting the corner of the corner detector ($\sqrt{2}\times4\times4.2''=23.7''$ off-axis). The sizes have been rounded up to 'nice' numbers (eg. 37.8 mm → 40 mm). (Values in Appendix)
- The radii of the Lyot stop has been set so that (using geometric optics) it illuminates 90 m of the primary mirror.

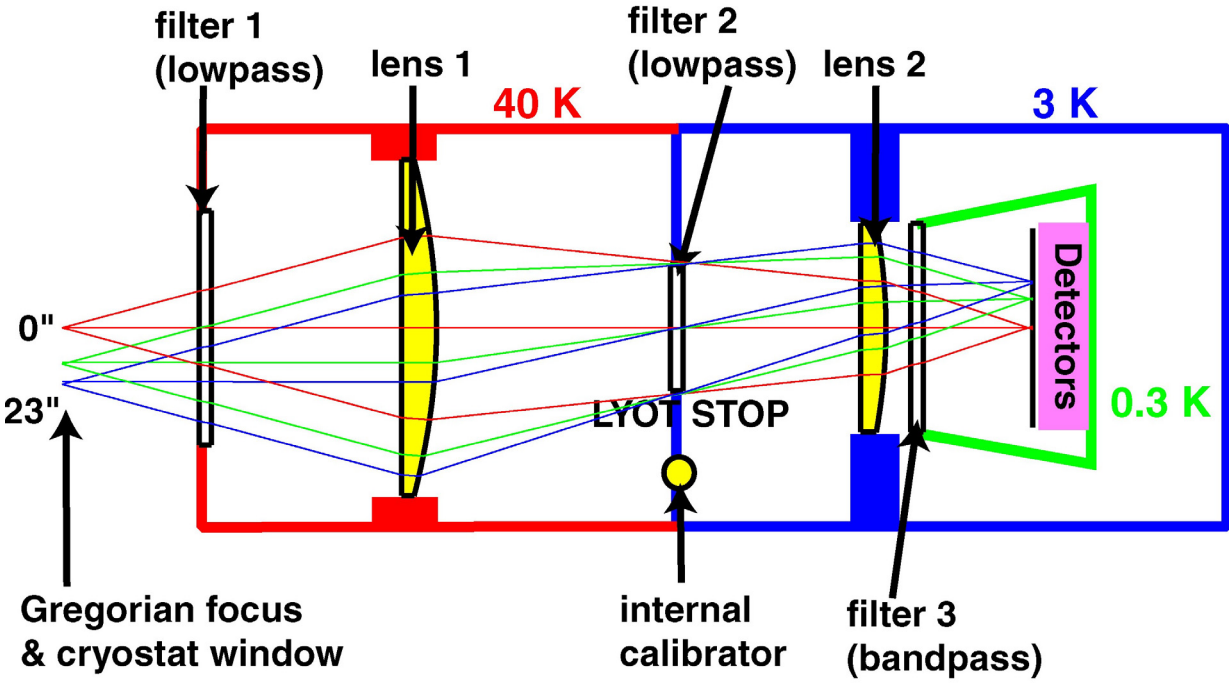

Figure 2. A schematic of the optical design.

Image quality

When designing the optics, the image quality was optimized simultaneously for rays 0″ to 34″ off-axis. 13 ray heights were used, concentrated below 23″ (where our detectors will be). To create a good Lyot stop the RMS differences between the rays at its edge were calculated and added to the error function used in optimization. Getting the weight of this term was important as it was often possible to sacrifice image quality for a perfect Lyot stop. During optimization the effective focal length was constrained to be 162,000 mm exactly. After optimization the image quality was evaluated at a grid of points across the array. All points less than 27″ off-axis were found to be diffraction limited to better than 1%. The finite size of the detectors causes far more change in the beam size (10 to 20%). The f# changes from f/1.595 in the center of the array to f/1.679 at the very edge.

Examples of spot diagrams and modulation transfer functions (MTFs) are shown in Figure 3. Code V was used to calculate the PSF using the geometric ray tracing approximation. Beam widths were ~8″ (FWHM) and the first side lobes were -17.7 dB down, 11.4″ from the center of the beam. Far out side lobes dropped to below -40 dB. These calculations are approximations

(due to the geometric ray tracing), better calculations were carried out using full diffraction (see below).

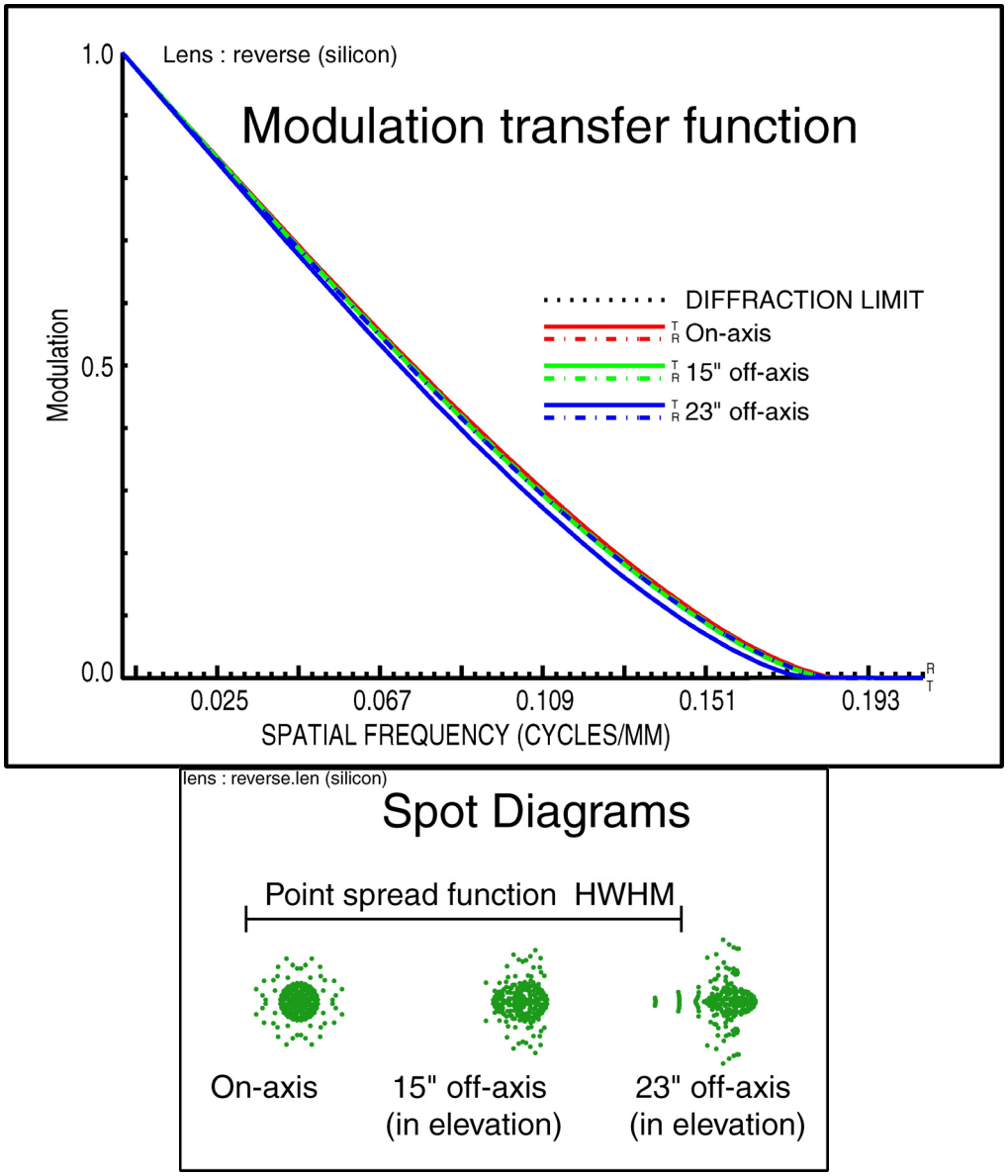

Figure 3. The spot diagrams and modulation transfer functions for rays 0, 15 and 23″ off-axis. The RMS spot diameters are 0.27, 0.29 and 0.35 mm respectively. The diffraction PSF has a FWHM of 6.6 mm. Some asymmetry can be seen in the 23″ MTF.

Tolerancing

To check that the design is not sensitive to misalignments and manufacturing errors, inverse tolerancing was used to determine how large the errors would have to be in order to produce an RMS wavefront error of 1% (a decrease in the gain of 1.6%). The results for the on-axis pixel are in Table 1. (Some of these errors are less than 1% because the quantity being investigated had a very small effect on the RMS and Code V hit an upper limit.) Other pixels were similar. Many parameters have little or no affect on image quality. If all the errors in the table are allowed to take a random value (with a uniform distribution) between zero and the values listed, the probable (97.7%) RMS wavefront error is 2.5%, a decrease in gain of 9.4%.

Quantity	Error	RMS wavefront error
Refractive index of lens	0.04	1.0%
Refractive index of filter	0.04	0.0%
Z position of lens 1	3 mm	0.7%
Z position of Lyot stop	3 mm	0.1%
Z position of lens 2	3 mm	0.1%
Z position of array	2.8 mm	1.0%
Fit of lens 1 to test plate	0.3 mm	0.8%
Fit of lens 2 to test plate	0.3 mm	0.5%
Tilt of lens 1	6°	0.1%
Tilt of lens 2	6°	0.2%
Y Shift of lens 1	10 mm	0% (image moved off-axis)
Y Shift of lens 2	10 mm	0% (image moved off-axis)
Tilt of receiver	6°	0.2%
Y Shift of receiver	10 mm	0% (image moved off-axis)
Z Shift of receiver	4.2 mm	1.0%

Table 1 : RMS errors in the wavefronts due to misalignments. Z shifts are along the optical axis and Y shifts perpendicular.

This process was then repeated, allowing the secondary mirror to be moved (up to 2 cm & 4°) to simulate the process of focusing the telescope – a process that will be needed anyway. With the exception of tilts and displacements of the lenses is possible to focus these errors out. The expected RMS wavefront error decreased to 0.6% (a reduction in gain of less then 1%). The maximum mirror movement was 11mm and .3°. This demonstrates that manufacture and assembly of the design should not be a problem and sub-millimeter alignment is not needed.

Predicted PSF and spillover

All the above tests use geometric ray tracing. To test the effects of diffraction, the Code V model was reversed so that the source was a point on the array and a perfect lens added after the primary mirror so that a perfect telescope (which would produce plane wavefronts) would image at a point when geometric optics is used for analysis. The stop was changed to be the Lyot stop. All aperture sizes were set to be the clear apertures listed in the Appendix.

To simulate the illumination of the stop by a flat black body (whose apparent area will decrease as the cosine of the angle from the axial direction), a .int file was then placed over a dummy surface centered on the point source. Geometric ray tracing was used to calculate the phase and amplitude of the illumination across the Lyot stop. It should be noted that as the detectors are of comparable size to the wavelength, this model may not be accurate, however when no .int file was used the results of these tests showed no significant difference.

The BPR option in Code V was then used to calculate the illumination of each surface from the Lyot stop onwards (using the apertures set above). BPR uses ray tracing to calculate the amplitude and phase on a reference sphere one side of a surface from the amplitude and phase of a similar reference sphere on the other. Full diffraction calculations are then used to calculate the illumination of one surface from the last. In these calculations Code V automatically chose the diffraction regime.

From the illumination of the secondary and primary mirrors spillover and beam patterns were calculated. These are shown in Table 2. Cross-sections of the illumination of the secondary and primary mirrors are shown in Figure 4. Both show that the illumination of the mirrors is well controlled and that ground or sky spillover will not be a problem.

Azimuth (″)	Elevation (″)	Spillover at Secondary	Spillover at primary
0	0	0.07%	0.24%
0	14.3	0.01%	0.07%
14.5	14.5	0.26%	0.33%

Table 2. Spillover from the mirrors calculated using BPR as a function of distance from the center of the array.

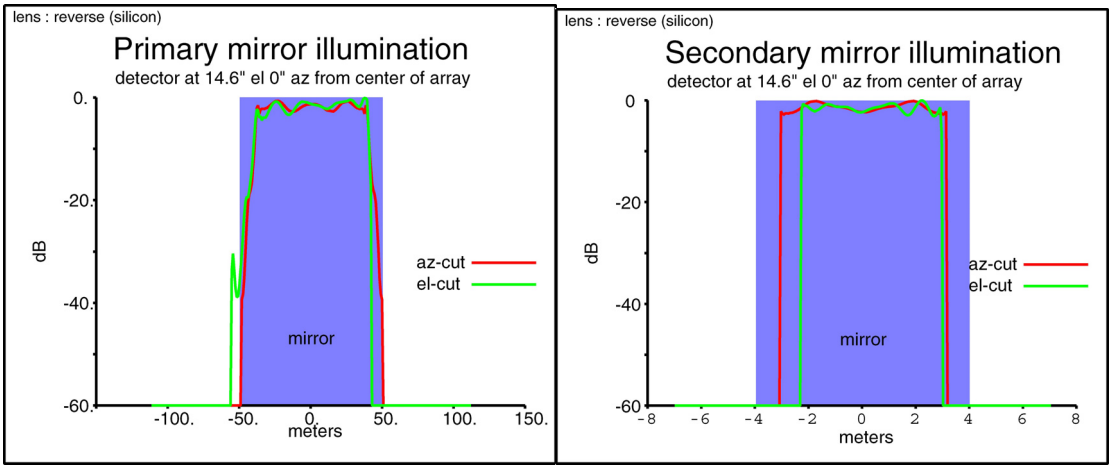

Figure 4. The illumination of the primary and secondary mirrors calculated using BPR.

By taking FFTs of the primary mirror illumination and convolving the result with the geometric image of a detector on the sky, beam patterns across the array were calculated. In order to obtain resolution, the primary was coarsely sampled in the center of a (2048×2048) FFT grid, (the largest my desktop could handle within Code V). Even so resolution was limited to 0.1″. Two examples are shown in Figure 5. FWHM were 7.9″ at the center of the array and 8.05″ at the edge, 1″ smaller than expected from a uniformly illuminated 90 m mirror (once detector size is taken into account). Typical first side lobes are -16 dB to -18 dB down (slightly higher than expected) and far out side lobes are -35 to -40 dB down. Side lobes decreased at the very edge of the array possibly due to rounding of the illumination pattern (the beam width also showed a slight decrease here to 7.7″ which would be consistent with this).

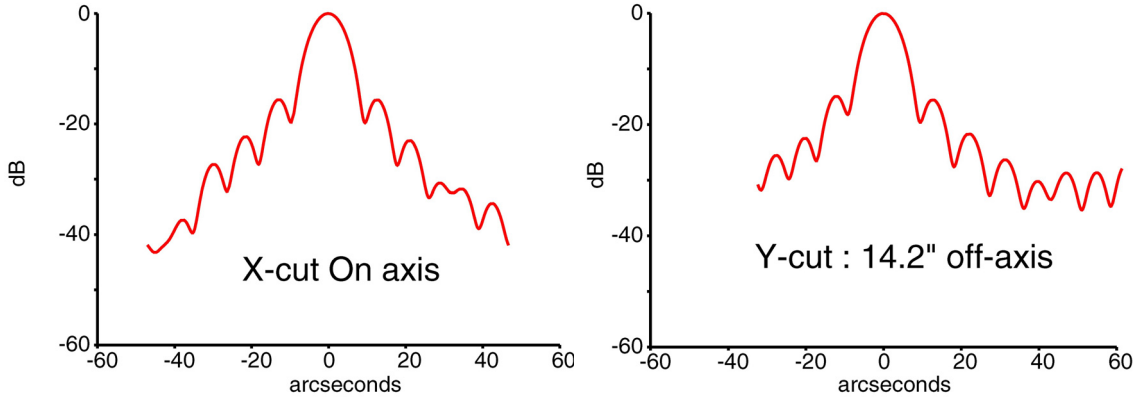

Figure 5 : Beam patterns calculated from FFTs of the primary mirror illumination. The results have been convolved with the detector's geometric image to take into account detector size.

Ghosting

The last check of the optics was to ensure stray light from reflections off surfaces does not cause any strong ghost images. Each surface was assigned a realistic reflectivity; 20% for the array and 2% for each lens or filter surface. It was assumed that the optics were in an optics box designed so that stray light is absorbed. The lens file, from the Gregorian window to a dummy surface at the array was turned into non-sequential surfaces and large edge apertures were added to each surface so that any rays that missed the clear aperture would be absorbed.

A surface near the array was made to reflect the first time a ray hits and refract the second time the same ray hits it, while another surface further from the array was made to refract first then reflect allowing Code V to model reflections between any pair of surfaces. An example where light is reflected from the array, travels out to the flat side of lens 2 before being reflected back to form an out-of-focus image is shown in Figure 6.

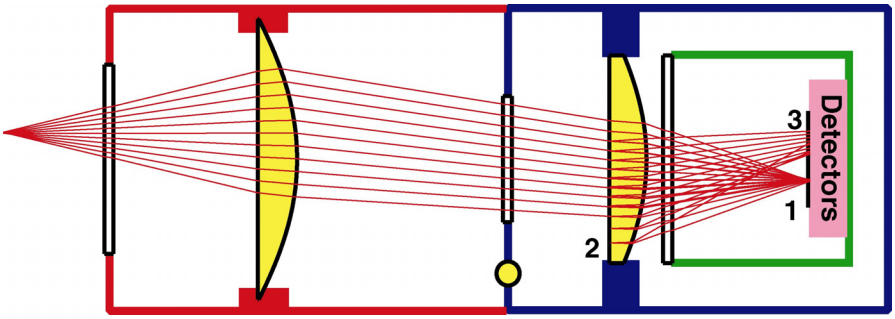

Figure 6. One of the most intense ghost images. Light is reflected off the array at 1. It hits the flat side of the second lens at 2. and creates an out-of-focus image at 3. This image is particularly strong as reflections from the array are 20% and all of this light is making it back to the array.

For each pair of surfaces the illumination of focal plane from a point source at infinity was calculated using Monte Carlo ray tracing with 10^5 rays (Code V's LUM function). The strength of the point source was set proportional to the combined reflectivity of the surfaces in question with allowances for losses at the additional number of surfaces that the rays must cross. Calculations for every pair of surfaces were added together to give the total ghost image. This was normalized by carrying out a LUM run without any surfaces reflecting and normalizing everything to the total power reaching the array. The ghost image was convolved with a 7.5″ FWHM Gaussian to approximate diffraction. If this was not done then power concentrated in sharp sub-diffraction sized peaks could have masked a diffuse but still bright ghost image.

The ghosting analysis program takes about an hour to run, and has been used both on and off axis. A cut through the ghost image from a source 15″ off-axis with a PSF (calculated using BEA above) superimposed on top is shown in Figure 7. As well as the total image there are plots showing the individual contributions of the different surfaces (grouped as to where the light is first reflected from). The highest image is 32 dB down but all this power comes from reflections within the filters. As a result this ghost image will always fall where the real image is and is not important. There is also a broad peak at -40 dB 12 to 38″ off-axis. With the current design this is still well below the PSF and so is not a problem, even should our estimated reflectivities be too low. However if lens 2 has its curved side away from the array this peak becomes much more

focused with a peak ~-29 dB (higher than some predicted diffraction side lobes). For this reason the less than ideal orientation of lens 2 was chosen.

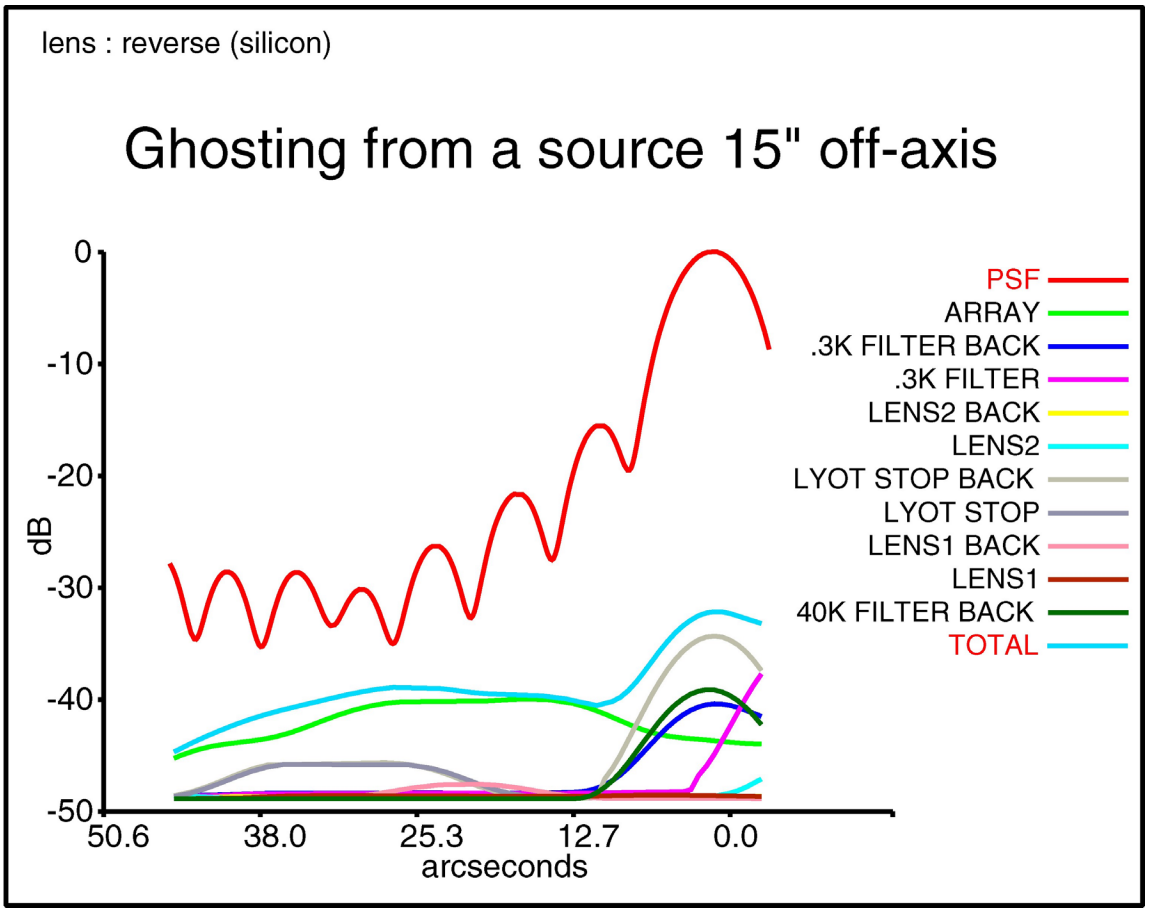

Figure 7. Ghost images created by reflections between pairs of surfaces. A PSF has been added to show that ghosting will not create any extra side lobes. Each line represents the image formed by light first reflected from a given surface.

Manufacture

A number of manufacturers have been found who can cut aspheric silicon lenses. Preliminary quotes have been of the order $3000 and cheaper manufacturers may be found once the final shapes are known. Due to thermal expansion, the parameters given to them will be slightly different from the parameters in the Appendix (which are what are required at cryogenic temperatures while the lenses are cut at room temperatures). Code V can calculate the differences.

The lenses are housed in an optics box mounted at the first lens only. Flexible cooling straps connect to the other stages. G10 tube connects the 40K and 3K parts, a 0.5 mil stainless steel foil makes this tube light-tight, and black baffles (a stycast/ silicon carbide paint) ensure stray light is absorbed. Again, the parts are cut at room temperatures to lengths calculated so that when they cool, the lenses/filters are apart by the lengths listed in the Appendix.

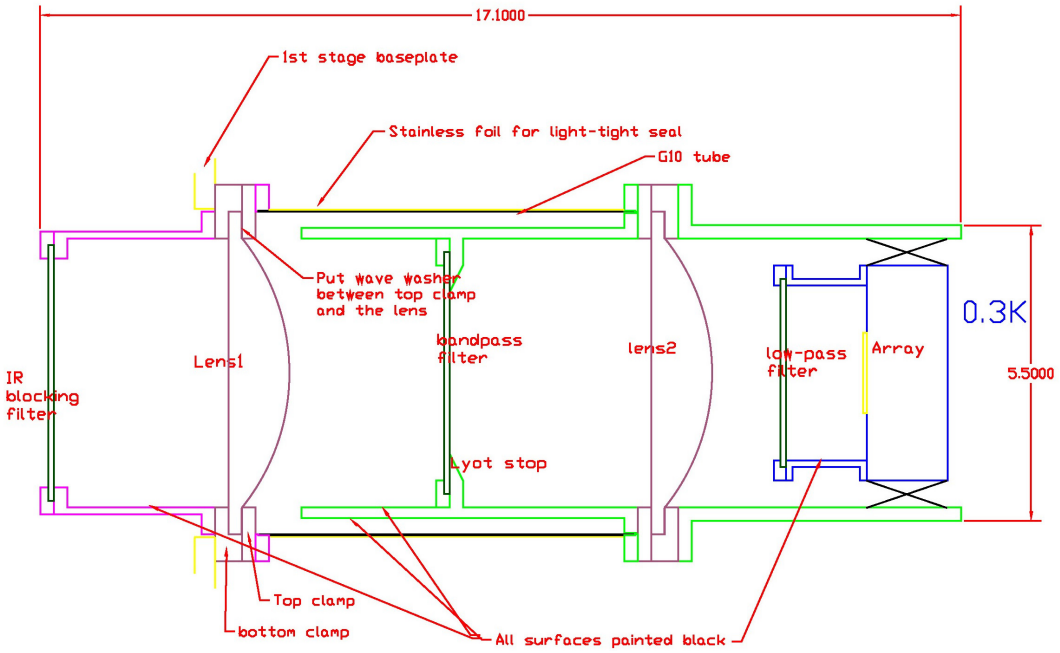

Figure 8 : The housing for a quartz version of the cold optics. The Silicon optics will have a similar housing. Sizes are in inches.

Conclusions

The silicon based optical design presented should produce diffraction limited beams across the entire 8×8 array, with pixel sizes of approximately 8″ (taking into account finite detector size). Spillover and side lobes (either from diffraction or stray light) should be below -30 dB beyond 25″ from the main beam). The First side lobes are -18 to -16 dB at around 11.7″ from the main beam in line with what is to be expected with typical fast edge tapers in the illumination of a primary mirror. All in all the design looks good, it easily fits in the cryostat and it should be possible to make at reasonable cost.

Appendix

Listed below are the parameters of the lenses in sequence file format:

S <surface number> <surface curvature> <distance to next surface> <material>.
SLB <surface name>

K,A,B,C,D represent the terms of the aspheric formula which gives the sag z in terms of h (the distance from the optical axis) and c (the curvature): $z = \frac{ch^2}{1+\sqrt{1-(1+K)c^2h^2}} + Ah^4 + Bh^6 + Ch^8 + Dh^{10}$

```
S 6     0.00000000      55.000000          'vac'
   SLB "Gregorian focus"

S 7     0.00000000      5.000000           'filter'
   SLB "40K filter"

S 8     0.00000000      76.525000          'vac'
   SLB "40K filter back"

S 9     0.00000000      14.083192          'silicon'
   SLB "lens1"

S 10    -0.00413441     94.170438          'vac'
   SLB "lens1 back"
   ASP
   K    -3.884782
   IC     YES      ;CUF    0.000000
   A  -.184951E-08   ;B  -.640385E-11   ;C  0.253747E-14   ;D  -.267786E-18

S 11    0.00000000      5.000000           'filter'
   SLB "Lyot stop"

S 12    0.00000000      71.531369          'vac'
   SLB "Lyot stop back"

S 13    0.00000000      10.185237          'silicon'
   SLB "lens2"

S 14    -0.00467100     10.000000          'vac'
   SLB "lens2 back"
   ASP
   K    -12.413004
   IC     YES      CUF:    0.000000
   A  0.891879E-08   ;B  -.142099E-09   ;C  0.992324E-13   ;D  -.219622E-16

S 15    0.00000000      5.000000           'filter'
   SLB ".3K filter"

S 16    0.00000000      44.069873          'vac'
   SLB ".3K filter back"

 ARRAY
```

The Apertures have the following radii (130% clear aperture):

Filter 1	45 mm
Lens 1	65 mm
Lyot stop	23.8 mm
Lens 2	40 mm
Filter 3	40 mm

This page is blank

This page is blank